Analysis of bifurcation and explosive amplitude death in a pair of oscillators coupled via time-delay connection

Keiji Konishi,[1,*] Koki Yoshida,[2] Yoshiki Sugitani,[1] and Naoyuki Hara[1]
[1]*Department of Electrical and Electronic Systems Engineering, Osaka Metropolitan University, 1-1 Gakuen-cho, Naka-ku, Sakai, Osaka 599-8531, Japan*
[2]*National Institute of Technology, Toyama College, 13 Hongo-machi, Toyama city, Toyama 939-8630, Japan*

(Received 20 October 2024; accepted 19 February 2025; published 10 March 2025)

Delay-induced amplitude death (AD) has received considerable research interest. Most studies on delay-induced AD investigated the local stability of equilibrium points. The present study examines the global dynamics of delay-induced AD in a pair of identical Stuart-Landau oscillators. Bifurcation diagrams consisting of synchronized periodic orbits and an equilibrium point are used to determine the mechanism of the emergence of delay-induced AD. It is shown that explosive delay-induced AD can occur via a Hopf bifurcation at the equilibrium point and a saddle-node bifurcation of synchronized periodic orbits when the delay time for the connection is continuously varied. The Hopf and saddle-node bifurcation curves in the coupling parameter space clarify the dependence of the coupling parameters on the global dynamics.

DOI: 10.1103/PhysRevE.111.034206

I. INTRODUCTION

Quenching phenomena, collective behaviors induced by mutual interactions in coupled oscillators [1,2], are classified into oscillation death (OD) or amplitude death (AD) based on their emergence mechanism [3–5]: OD is the emergence of stable inhomogeneous equilibrium points and AD is the stabilization of an equilibrium point embedded within isolated oscillators. AD has been widely studied in the field of engineering because its noninvasiveness is useful for suppressing harmful oscillations and for maintaining such suppression with a tiny amount of coupling energy in two or more man-made systems that interact, such as thermoacoustic systems [6–12] and DC microgrids [13]. However, the simplest and easiest-to-implement noninvasive diffusive coupling never induces AD in coupled identical oscillators [14,15]. Considerable attention has been paid to modified noninvasive diffusive couplings, which can induce AD in coupled identical oscillators [4,5,16].

Among modified diffusive couplings, delay coupling [17–19] has become important because it describes the situation where two or more systems mutually interact via signals with finite propagation speed. AD induced by delay coupling has thus been extensively studied [5,16] from viewpoints such as suppression of harmful oscillations in thermoacoustic systems [6–12], development of delay coupling [20–26], and application to networks [27–36].

To broaden the range of applications of delay-induced AD, the coupling parameters (i.e., coupling strength and delay time) that induce death have to be appropriately chosen based on the stability of death. However, such stability cannot be easily analyzed, since the dynamics of delay-induced AD is subject to both nonlinearity and time delay. The nonlinearity prevents the use of linear stability analysis, which is well established in control theory, and the time delay makes it difficult to analyze the stability of the dynamics, which is the same as the analysis of functional differential equations. Nevertheless, for the local stability of equilibrium points in coupled oscillators, linear stability analysis can be used without regard to nonlinearity. Although time-delay linear systems that describe the local stability of equilibrium points have characteristic functions described by quasipolynomial equations with infinitely many roots, such systems can be analyzed based on the behavior of the rightmost root with respect to the delay time. Most stability analyses of delay-induced AD have thus focused on the local stability of equilibrium points [27–34]. In contrast, few attempts have been made to analyze the global dynamics of delay-induced AD. This means that the dynamics far from equilibrium points is still unclear and the mechanism of the emergence of delay-induced AD is not fully understood from the viewpoint of the bifurcation of periodic orbits.

Growing attention has recently been given to explosive AD/OD, a discontinuous and irreversible transition from the oscillatory state to AD/OD, that occurs when a coupling parameter is continuously varied. Bi *et al.* were the first to report that explosive OD occurs in Stuart-Landau (SL) oscillators with a frequency distribution that are connected via frequency-distributed coupling [37]. Verma *et al.* found that explosive nontrivial AD, a stabilization of the homogeneous equilibrium point that depends on coupling, occurs in identical oscillators coupled via mean-field diffusion [38]. It was later reported that explosive AD/OD can be induced by several types of coupling, including conjugate variable coupling [39–41], common environment coupling [42–44], dynamical agents coupling [45], mean-field coupling [46–48], nondiffusive global coupling [49], mixed attractive-repulsive coupling [50], and diffusive coupling with a low-pass filter [51,52]. Recently, Hui *et al.* experimentally demonstrated explosive

[*]https://www.omu.ac.jp/eng/ees-ecs

death in real electrical circuits [52]. Although explosive death has been extensively investigated for various types of coupling, few studies have focused on delay coupling despite its importance.

The present study examines the global dynamics of AD in a pair of identical SL oscillators coupled via a time-delay connection. Most studies on delay-induced AD considered a simple SL oscillator whose frequency does not depend on amplitude. In contrast, the present study employs the more general SL oscillator [53,54] whose frequency depends on amplitude. We derive periodic orbits synchronized in phase and antiphase and examine their stability. Bifurcation diagrams consisting of the derived orbits are used to examine the influence of the frequency dependency on the synchronized periodic orbits and to determine the mechanism of the emergence of AD. The bifurcation diagrams show that explosive AD can occur via a Hopf bifurcation of the equilibrium point and a saddle-node bifurcation of synchronized periodic orbits when the delay time is continuously varied. Furthermore, we obtain the Hopf and saddle-node bifurcation curves in the coupling parameter space. These curves clarify the dependence of the coupling parameters on the global dynamics.

II. DELAY-COUPLED OSCILLATORS

In this section, we briefly review a SL oscillator whose frequency depends on amplitude and provide the stable range for the delay time for the equilibrium point in the delay-coupled SL oscillators. Some numerical examples show that even if the equilibrium point is locally stable, there are cases where AD fails to occur.

A. Stability analysis of equilibrium point

We review the dynamics of a single SL oscillator [53,54] with two parameters, namely $\omega > 0$ and $b \in \mathbb{R}$:

$$\dot{Z}(t) = F[Z(t), b], \tag{1a}$$

$$F[Z(t), b] := \{1 + \mathrm{i}\omega - (1 + \mathrm{i}b)|Z(t)|^2\}Z(t), \tag{1b}$$

where $Z(t) \in \mathbb{C}$ is the state variable and $\mathrm{i} := \sqrt{-1}$ denotes the imaginary unit. Oscillator (1) with $Z(t) = r(t)\exp(\mathrm{i}\theta(t))$ can be expressed in polar coordinates as

$$\dot{r}(t) = \{1 - r(t)^2\}r(t), \tag{2a}$$

$$\dot{\theta}(t) = \omega - br(t)^2, \tag{2b}$$

where $r(t) \geqslant 0$ and $\theta(t) \in \mathbb{R}$ are the amplitude and angle variables for $Z(t)$, respectively. Oscillator (1) has an unstable equilibrium point $r(t) = 0$ [i.e., $Z(t) = 0$] and a stable limit cycle with amplitude $r(t) = 1$ [i.e., $|Z(t)| = 1$]. The parameter ω is the rotation velocity of $\theta(t)$ around the unstable equilibrium point. The parameter b describes how the rotation velocity depends on the amplitude $r(t)$. The rotation velocity on the stable limit cycle $r(t) = 1$ is given by $\dot{\theta}(t) = \omega - b$. Note that there are three cases, namely $b = 0$, $b > 0$, and $b < 0$. For $b = 0$, we see that the velocity $\dot{\theta}(t) = \omega$ does not depend on amplitude $r(t)$. In contrast, for $b > 0$ ($b < 0$), the velocity $\dot{\theta}(t) = \omega - br(t)^2$ decreases (increases) with increasing $r(t)$. In other words, for $b > 0$, the velocity $\dot{\theta}(t)$ inside the limit cycle [i.e., $r(t) < 1$] is higher than that on the limit cycle $r(t) = 1$; on the other hand, the velocity outside the limit cycle [i.e., $r(t) > 1$] is lower than that on the limit cycle. For $b < 0$, the velocity inside (outside) the limit cycle is lower (higher) than that on the limit cycle.

Now, we consider a pair of SL oscillators coupled via a time-delay connection with coupling strength $K \geqslant 0$ and delay time $\tau \geqslant 0$:

$$\dot{Z}_1(t) = F[Z_1(t), b] + K\{Z_2(t - \tau) - Z_1(t)\}, \tag{3a}$$

$$\dot{Z}_2(t) = F[Z_2(t), b] + K\{Z_1(t - \tau) - Z_2(t)\}, \tag{3b}$$

where $Z_j(t) \in \mathbb{C}$ is the state variable for oscillator $j \in \{1, 2\}$. It should be emphasized that most studies on delay-induced AD in coupled SL oscillators dealt with only the case of $b = 0$ [29–35]. Coupled oscillators (3) have the following equilibrium point:

$$Z_1(t) = Z_2(t) = 0, \tag{4}$$

independently of b. The local dynamics of equilibrium point (4) is equivalent to that of the linear system,

$$\dot{z}_1(t) = (1 + \mathrm{i}\omega)z_1(t) + K\{z_2(t - \tau) - z_1(t)\}, \tag{5a}$$

$$\dot{z}_2(t) = (1 + \mathrm{i}\omega)z_2(t) + K\{z_1(t - \tau) - z_2(t)\}, \tag{5b}$$

where $z_j(t) \in \mathbb{C}$ is a small perturbation of oscillator $j \in \{1, 2\}$ around point (4). The characteristic function,

$$\begin{aligned} g(s) := &\{s - 1 - \mathrm{i}\omega + K(1 - e^{-s\tau})\} \\ &\cdot \{s - 1 - \mathrm{i}\omega + K(1 + e^{-s\tau})\}, \end{aligned} \tag{6}$$

governs the stability of a linear system (5). On the basis of function (6), we can analytically obtain the Hopf bifurcation points for τ as follows:

$$\tau_\pm(\ell) = \begin{cases} \dfrac{\pm\psi(K)/2 + \ell\pi}{\omega \pm \sqrt{2K - 1}} & \text{if } 1/2 \leqslant K \leqslant 1 \\[2ex] \dfrac{\mp\psi(K)/2 + (\ell \pm 1)\pi}{\omega \pm \sqrt{2K - 1}} & \text{if } 1 \leqslant K \end{cases}, \tag{7}$$

where ℓ is an integer and $\psi(K) \in [0, \pi]$ is given by

$$\psi(K) := \cos^{-1}\frac{K^2 - 4K + 2}{K^2}. \tag{8}$$

The root of function (6) passes the imaginary axis from left (right) to right (left) at $\tau = \tau_+(\ell)$ [$\tau = \tau_-(\ell)$] with increasing τ. We can easily obtain the stable ranges for τ based on the direction of the root passing the imaginary axis and the function (6) having one unstable root at $\tau = 0$ for $K \geqslant 1/2$. These analytical results were obtained in previous studies (e.g., see Ref. [55]). It should be noted that linear system (5) does not depend on parameter b; thus, a local stability analysis of equilibrium point (4) for $b = 0$, which has been conducted in previous studies [29–35], is valid even for $b \neq 0$.

B. Numerical example

We now examine the stability of equilibrium point (4) using numerical simulations. We set the parameters ($\omega = 10$ and $K = 5$) and derive the stable range for $\tau \in (\tau_-(1), \tau_+(0))$ with $\tau_-(1) = 0.0919$ and $\tau_+(0) = 0.1922$. The delay time is fixed at $\tau = 0.15$, which is within the stable range. Figures 1(a)–1(c) show time series data for $\mathrm{Re}[Z_{1,2}(t)]$ for

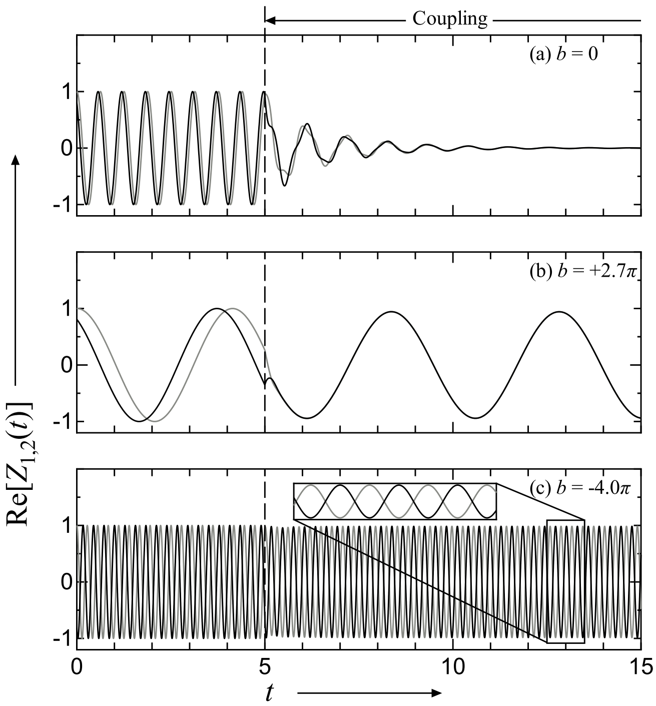

FIG. 1. Time series data for $\mathrm{Re}[Z_{1,2}(t)]$ for coupled oscillator (3) with $\omega = 10$, $K = 5$, and $\tau = 0.15$ for (a) $b = 0$, (b) $b = +2.7\pi$, and (c) $b = -4.0\pi$.

coupled oscillator (3) for b values of 0, $+2.7\pi$, and -4.0π, respectively. The oscillators behave independently without coupling (i.e., $K = 0$) for $t \in [0, 5)$ and are coupled at $t = 5$. After coupling, the behavior of the state variables changes as follows: for $b = 0$, the state variables converge on equilibrium point (4); for $b = +2.7\pi$, the state variables are synchronized in phase with low frequency; for $b = -4.0\pi$, the state variables are synchronized in antiphase with high frequency. As can be seen, with locally stable equilibrium point (4), AD occurs for $b = 0$ but fails to occur for $b = +2.7\pi$ and $b = -4.0\pi$. The main aim of the present study is to clarify the global dynamics to understand the failure of AD induction.

III. BIFURCATION DIAGRAMS

This section explains the failure of the AD induction described above using bifurcation diagrams consisting of periodic orbits in coupled oscillators (3), their stability, and $\tau_\pm(\ell)$ in Eq. (7).

A. Synchronized periodic orbits and their stability

We now derive the synchronized periodic orbits for coupled oscillators (3) and provide a procedure for classifying their stability based on previous studies [35,56]. Coupled oscillators (3) in polar coordinates with $Z_{1,2}(t) = r_{1,2}(t)\exp(\mathrm{i}\theta_{1,2}(t))$ can be expressed as

$$\dot{r}_{1,2}(t) = \{1 - K - r_{1,2}(t)^2\}r_{1,2}(t) + K r_{2,1}(t-\tau)\cos\{\theta_{2,1}(t-\tau) - \theta_{1,2}(t)\}, \tag{9a}$$

$$\dot{\theta}_{1,2}(t) = \omega - b r_{1,2}(t)^2 + K\frac{r_{2,1}(t-\tau)}{r_{1,2}(t)}\sin\{\theta_{2,1}(t-\tau) - \theta_{1,2}(t)\}. \tag{9b}$$

We focus on the situation where the two oscillators are synchronized in phase ($m = 0$) or antiphase ($m = 1$) as follows:

$$r_{1,2}(t) = R, \quad \theta_1(t) = \Omega t, \quad \theta_2(t) = \Omega t + m\pi, \tag{10}$$

where $R > 0$ and $\Omega > 0$ are, respectively, the common amplitude and frequency. Substituting synchronized state (10) into coupled oscillators (9) yields

$$R^2 = 1 - K(1 - \cos\Omega\tau\cos m\pi) > 0, \tag{11a}$$

$$\Omega = \omega - bR^2 - K\sin\Omega\tau\cos m\pi. \tag{11b}$$

If (τ, K) satisfies Eq. (11) for $m = 0$ ($m = 1$), then the in-phase (antiphase) synchronized state (10) exists.

To check the stability of synchronized state (10), coupled oscillators (9) are linearized around state (10) satisfying Eq. (11) as follows:

$$\dot{\boldsymbol{X}}(t) = \begin{bmatrix} \boldsymbol{A} & \boldsymbol{0} \\ \boldsymbol{0} & \boldsymbol{A} \end{bmatrix}\boldsymbol{X}(t) + \begin{bmatrix} \boldsymbol{0} & \boldsymbol{B} \\ \boldsymbol{B} & \boldsymbol{0} \end{bmatrix}\boldsymbol{X}(t-\tau), \tag{12}$$

where

$$\boldsymbol{X}(t) := [\Delta r_1(t) \quad \Delta\theta_1(t) \quad \Delta r_2(t) \quad \Delta\theta_2(t)]^\top,$$

$$\boldsymbol{A} := \begin{bmatrix} -R_\mathrm{K} - 2R^2 & R\Omega_\mathrm{R} \\ -\Omega_\mathrm{R}/R - 2bR & -R_\mathrm{K} \end{bmatrix},$$

$$\boldsymbol{B} := \begin{bmatrix} R_\mathrm{K} & -R\Omega_\mathrm{R} \\ \Omega_\mathrm{R}/R & R_\mathrm{K} \end{bmatrix},$$

$$\Delta r_1(t) := r_1(t) - R, \quad \Delta r_2(t) := r_2(t) - R,$$

$$\Delta\theta_1(t) := \theta_1(t) - \Omega t, \quad \Delta\theta_2(t) := \theta_2(t) - \Omega t - m\pi,$$

$$R_\mathrm{K} := R^2 - 1 + K, \quad \Omega_\mathrm{R} := \Omega - \omega + bR^2.$$

The characteristic function for linear system (12),

$$F(s) := \det\begin{bmatrix} s\boldsymbol{I}_2 - \boldsymbol{A} & -\boldsymbol{B}e^{-s\tau} \\ -\boldsymbol{B}e^{-s\tau} & s\boldsymbol{I}_2 - \boldsymbol{A} \end{bmatrix}, \tag{13}$$

always has one zero root $s = 0$ [i.e., $F(0) = 0$], which corresponds to the synchronization manifold. Synchronized state (10) is locally stable if and only if function (13) does not have roots with a positive real part except the zero root. The stability of retarded-type linear time-delay systems, such as system (12), can be analyzed using the software tool `eigAM` [57].

B. Bifurcation diagrams for τ

Let us consider the bifurcation diagram consisting of equilibrium point (4), the common amplitude R and frequency Ω versus τ on the basis of the Hopf bifurcation point $\tau_\pm(\ell)$ given by Eq. (7), synchronized state (10) satisfying Eq. (11), and their stability obtained by analyzing function (13). The procedure for plotting R^2 and Ω in the diagram with fixed ω, b, and K is as follows: for a given $\tau \geqslant 0$, R^2 and Ω that satisfy Eq. (11) are obtained; for the obtained R^2 and Ω, the stability of the synchronized orbits is classified using function (13); R^2 and Ω (with information on their stability) are plotted; the above procedure is repeated for various values of τ. In addition, equilibrium point (4) is plotted with consideration of the stable ranges for τ obtained in Sec. II A.

The bifurcation diagrams for $b = 0$, $b = +2.7\pi$, and $b = -4.0\pi$ obtained using the above procedure are shown in Figs. 2(a)–2(c), respectively. The bold (thin) black line represents stable (unstable) point (4). The white filled squares (circles) are the Hopf bifurcation points $\tau_+(\ell)$ with $\ell \in \{0, 1\}$ [$\tau_-(\ell)$ with $\ell = 1$]. The bifurcation diagram for point (4) does not depend on b. The blue (red) lines denote R^2 and Ω for in-phase (antiphase) synchronized periodic orbits; the bold (thin) lines define stable (unstable) periodic orbits.

For $b = 0$ [see Fig. 2(a)], the in-phase (antiphase) stable synchronized periodic orbit is connected to the supercritical Hopf bifurcation point $\tau_-(1)$ [$\tau_+(0)$] which is an edge of the stable range for τ. The behavior of the time series data in Fig. 1(a) before coupling $t \in [0, 5)$ corresponds to the black filled circle at $R^2 = 1$ with symbol (A). The behavior after coupling $t \geqslant 5$ corresponds to the dotted line. The state variables then converge on point (4), represented by the black filled square.

For $b = +2.7\pi$ ($b = -4.0\pi$), as shown in Fig. 2(b) [Fig. 2(c)], the in-phase (antiphase) unstable synchronized periodic orbit is connected to the subcritical Hopf bifurcation point $\tau_-(1)$ [$\tau_+(0)$], which is an edge of the stable range for τ. The in-phase (antiphase) unstable orbit is also connected to the in-phase (antiphase) stable orbit with the common frequency Ω, which is much lower (higher) than the natural frequency $\omega = 10$, via the saddle-node bifurcation indicated by the orange (green) cross. The behavior in Fig. 1(b) [Fig. 1(c)] after coupling $t \geqslant 5$ corresponds to the black filled circle at $R^2 = 0.8873$ ($R^2 = 0.9709$) on the in-phase (antiphase) stable orbit. As can be seen, the reason AD fails to occur for $b = +2.7\pi$ ($b = -4.0\pi$) in Fig. 1(b) [Fig. 1(c)] is that the state variables converge on the in-phase (antiphase) stable synchronized periodic orbit with a low (high) common frequency.[1] Furthermore, the shape of the bifurcation diagram shows that no synchronized periodic orbits exist that prevent AD from occurring if τ is chosen from the range between the saddle-node bifurcation point and the supercritical Hopf bifurcation point $\tau_+(0)$ [$\tau_-(1)$].

IV. EXPLOSIVE AMPLITUDE DEATH

This section shows that explosive AD, a discontinuous and irreversible transition from the oscillatory state to AD, can occur in coupled oscillators (3) when the delay time τ is continuously varied. Let us define the average amplitude Z_R of $|Z_1(t)|^2$ and $|Z_2(t)|^2$ at $t = 500$ after transient behavior disappears:

$$Z_R := \frac{1}{2}\{|Z_1(500)|^2 + |Z_2(500)|^2\}. \tag{14}$$

Figures 3(a)–3(c) show Z_R versus the delay time $\tau \in [0, 0.5]$ for b values of 0, $+2.7\pi$, and -4.0π, respectively. The black

[1]It should be noted that depending on the phase difference at $t = 5$, the state variables may not converge on the stable synchronized periodic orbit.

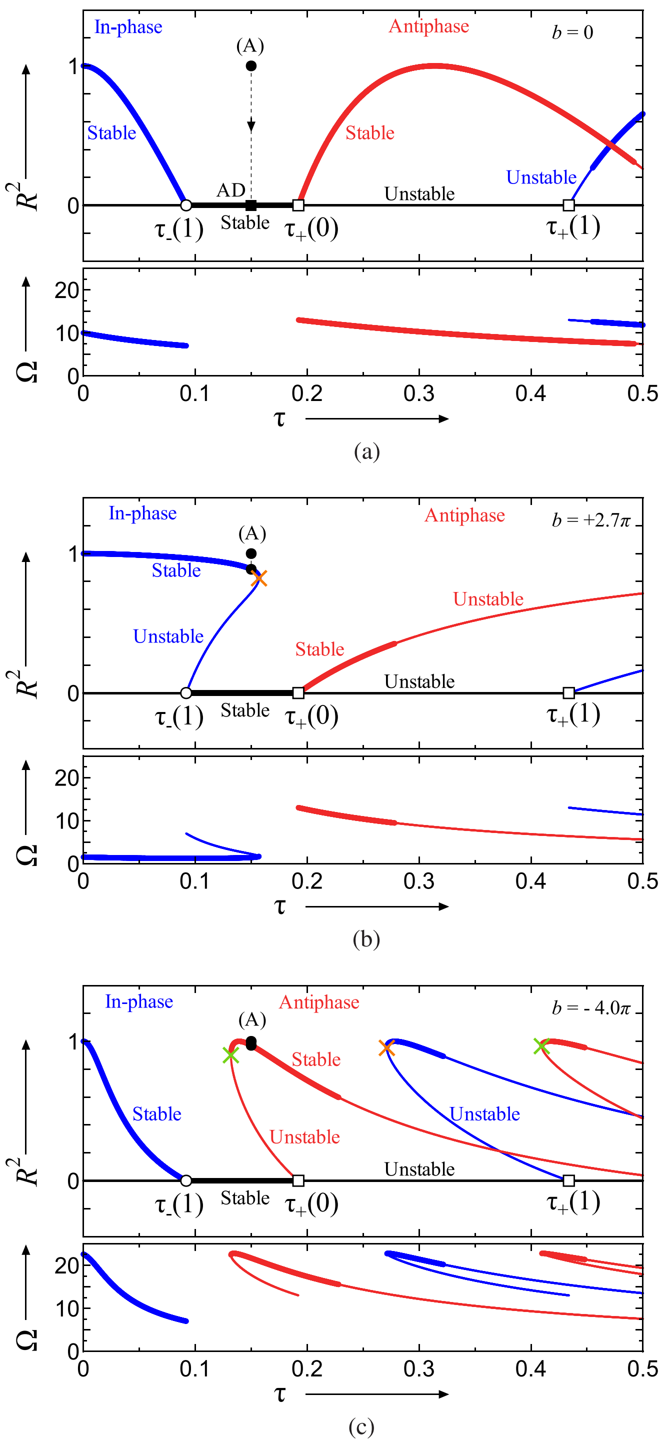

FIG. 2. Bifurcation diagrams for common amplitude R and frequency Ω for synchronized periodic orbits and equilibrium point (4) with $\omega = 10$ and $K = 5$ versus delay time $\tau \in [0, 0.5]$ for (a) $b = 0$, (b) $b = +2.7\pi$, and (c) $b = -4.0\pi$. The black lines represent point (4). The blue (red) lines denote R^2 and Ω for in-phase (antiphase) synchronized periodic orbits. The bold (thin) lines represent a stable (unstable) state. The orange (green) cross defines the saddle-node bifurcation point for in-phase (antiphase) synchronized periodic orbits.

circles (red crosses) represent Z_R as τ increases from 0 to 0.5 (decreases from 0.5 to 0). The initial condition for coupled oscillators (3) at a certain value of τ for black circles

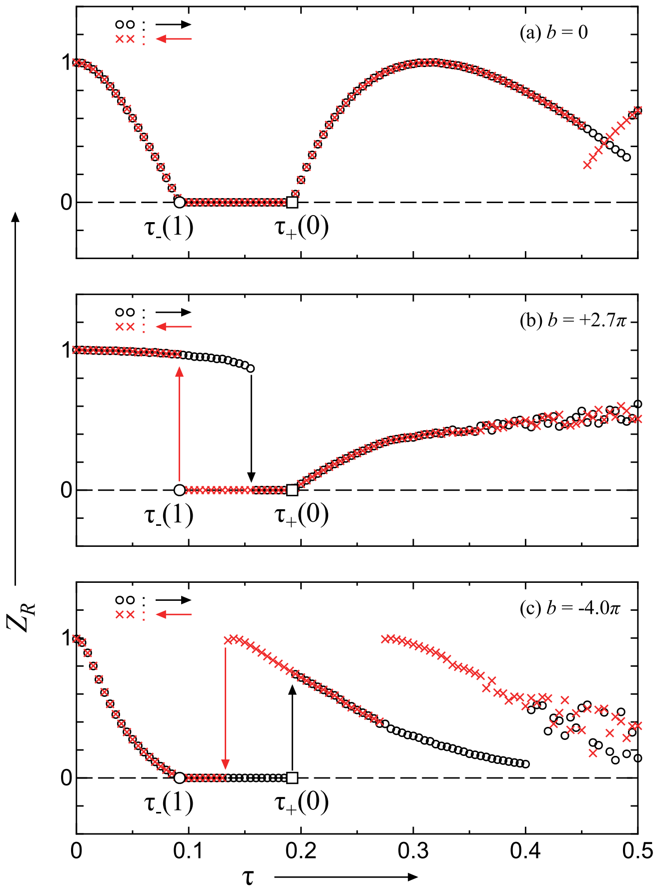

FIG. 3. Average amplitude Z_R with $\omega = 10$ and $K = 5$ plotted versus delay time $\tau \in [0, 0.5]$ for (a) $b = 0$, (b) $b = +2.7\pi$, and (c) $b = -4.0\pi$. The black circles (red crosses) represent forward (backward) continuation of Z_R with variation of τ.

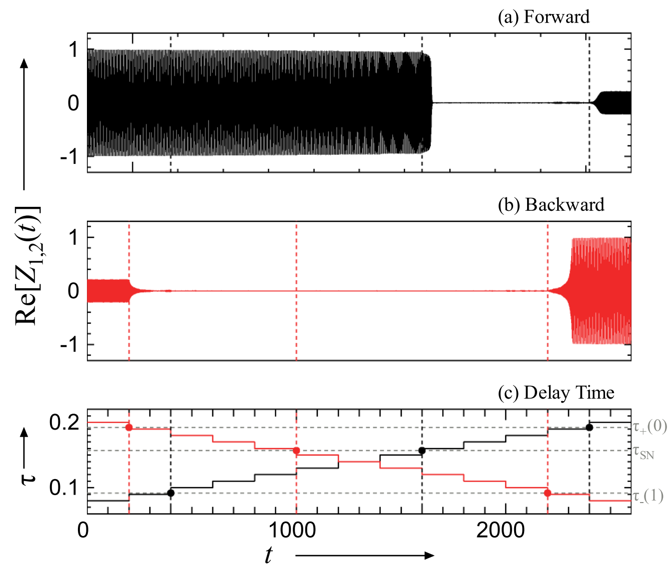

FIG. 4. Time series data for $\mathrm{Re}[Z_{1,2}(t)]$ and delay time τ for $b = +2.7\pi$ [see Figs. 2(b) and 3(b)]. The delay time τ slowly increases (decreases) stepwise with time from $\tau = 0.08 < \tau_-(1)$ to $\tau = 0.20 > \tau_+(0)$ [$\tau = 0.20 > \tau_+(0)$ to $\tau = 0.08 < \tau_-(1)$]. For increasing (decreasing) τ, the state variables and delay time are respectively plotted by the black (red) line in (a) and (c) [(b) and (c)].

(red crosses) is set to the trajectory[2] for $t \in [500 - \tau, 500]$ at $\tau - \Delta\tau$ (at $\tau + \Delta\tau$), where $\Delta\tau = 0.005$ is the step size for τ.

For $b = 0$ [see Fig. 3(a)], we focus on the stable range for τ between $\tau_-(1)$ and $\tau_+(0)$. The transitions from oscillatory states with $Z_R > 0$ to AD with $Z_R = 0$ are continuous and reversible. This means that explosive AD does not occur for $b = 0$. This is analytically proved in Sec. V and Appendix. In contrast, as shown in Fig. 3(b) [Fig. 3(c)], for $b = +2.7\pi$ ($b = -4.0\pi$), the transition is continuous and reversible around $\tau_+(0)$ [$\tau_-(1)$], but discontinuous and irreversible around $\tau_-(1)$ [$\tau_+(0)$], where hysteresis occurs. We see that explosive AD occurs for $b = +2.7\pi$ and -4.0π.

The mechanism of the emergence of explosive AD is illustrated in Fig. 2. For $b = 0$, the bifurcation diagram in Fig. 2(a) shows that the stable synchronized periodic orbits are connected to the supercritical Hopf bifurcation points $\tau_-(1)$ and $\tau_+(0)$, the edges of the stable range for τ. In contrast, for $b = +2.7\pi$ ($b = -4.0\pi$), as shown in Fig. 2(b) [Fig. 2(c)], the unstable synchronized periodic orbit, which is connected to the saddle-node bifurcation point, is also connected to the subcritical Hopf bifurcation point $\tau_-(1)$ [$\tau_+(0)$], an edge of the stable range for τ. The bifurcation diagram in Fig. 2 clearly explains why explosive AD emerges for $b = +2.7\pi$ and $b = -4.0\pi$, but not for $b = 0$. Based on the results, explosive AD occurs because the saddle-node bifurcation point $\tau = \tau_{SN}$ is within the stable range for τ; that is, $\tau_-(1) < \tau_{SN} < \tau_+(0)$.

In order to confirm the mechanism from the viewpoint of the time series data, $\mathrm{Re}[Z_{1,2}(t)]$ is plotted against time t in Figs. 4(a) and 4(b). Let us focus on the case of $b = +2.7\pi$ as an example [see Figs. 2(b) and 3(b)]. We consider two situations: the delay time τ slowly increases (decreases) stepwise with time from $\tau = 0.08 < \tau_-(1)$ to $\tau = 0.20 > \tau_+(0)$ [$\tau = 0.20 > \tau_+(0)$ to $\tau = 0.08 < \tau_-(1)$]. For increasing τ [black lines in Figs. 4(a) and 4(c)], the following observations can be made: the state variables behave in an oscillatory manner until $\tau = \tau_{SN}$; the state variables suddenly stop oscillating and converge on equilibrium point (4) [i.e., $Z_1(t) = Z_2(t) = 0$] at around $\tau = \tau_{SN}$; the state variables remain at the equilibrium point until $\tau = \tau_+(0)$ and then gradually start to oscillate at around $\tau = \tau_+(0)$. For decreasing τ [red lines in Figs. 4(b) and 4(c)], the following observations can be made: the state variables gradually stop oscillating and converge on the equilibrium point at around $\tau = \tau_+(0)$; the state variables remain at the equilibrium point until $\tau = \tau_-(1)$ and then suddenly start to oscillate at around $\tau = \tau_-(1)$; the state variables continue to oscillate after $\tau = \tau_-(1)$. These observations are consistent with the mechanism based on the bifurcation diagram in Fig. 2(b) and the average amplitude Z_R in Fig. 3(b).

V. BIFURCATION CURVES IN τ-K SPACE

This section extends the discussion on bifurcation diagrams with fixed K in Secs. III and IV to bifurcation curves in τ-K space. The curves for Hopf bifurcation were obtained

[2]In order to slightly perturb the coupled oscillators, Gaussian noise with a variance of 10^{-4} and zero mean is added to Eq. (3).

using Eq. (7). The curves for the saddle-node bifurcation of the periodic orbits, which play an important role in inducing explosive AD, are derived below based on a procedure for delayed feedback control systems [58].

Now, we focus on the synchronized state (10) (in phase or antiphase), which satisfies Eq. (11). Eliminating R^2 in Eq. (11), we have $\Omega = f(\Omega)$, where

$$f(\Omega) := \omega - b + K\{b(1 - \cos\Omega\tau \cos m\pi) - \sin\Omega\tau \cos m\pi\}. \tag{15}$$

The saddle-node bifurcation for periodic orbits occurs when two periodic orbits merge and disappear; thus, bifurcation occurs when Ω touches $f(\Omega)$ [i.e., $df(\Omega)/d\Omega = 1$] under inequality (11a).[3] This allows us to obtain τ and Ω at the saddle-node bifurcation point, which satisfy

$$0 = \tau(\omega - \Omega - b)(b\sin\Omega\tau - \cos\Omega\tau)\cos m\pi - b(\cos\Omega\tau\cos m\pi - 1) - \sin\Omega\tau\cos m\pi. \tag{16}$$

In addition, K is given by

$$K = \frac{1}{\tau(b\sin\Omega\tau - \cos\Omega\tau)\cos m\pi}. \tag{17}$$

As a consequence, τ, K, and Ω at the saddle-node bifurcation can be obtained from Eqs. (16) and (17) under inequality (11a) and $K \geqslant 0$. Note that for $b = 0$, it is easy to guarantee that the saddle-node bifurcation does not occur if $K > \tau - 1$ holds (see Appendix). This shows that the saddle-node bifurcation never occurs for any $\tau \in [0, 1)$ under $K \geqslant 0$.

Figures 5(a)–5(c) show the bifurcation curves and the stable region for equilibrium point (4) in coupling parameter space (τ, K) with $\omega = 10$ for b values of 0, $+2.7\pi$, and -4.0π, respectively. The bold (thin) black lines represent the Hopf bifurcation curves $\tau_-(\ell)$ [$\tau_+(\ell)$] analytically obtained using Eq. (7). The gray area is the stable region for equilibrium point (4). These Hopf bifurcation curves and the stable region do not depend on b. The orange (green) lines represent the saddle-node (denoted SN) bifurcation curves for in-phase (antiphase) synchronized periodic orbits, which were derived using the procedure described above. The bifurcation diagrams in Figs. 2(a)–2(c) correspond to the horizontal dotted lines at $K = 5$ in Figs. 5(a)–5(c), respectively. The behavior of the time series data in Fig. 1 corresponds to the black filled circle labeled (A) in Fig. 5.

For $b = 0$ [see Fig. 5(a)], we see that saddle-node bifurcation curves do not exist. This shows that explosive AD does not occur for any $\tau \in [0, 0.5]$ and $K \in [0, 8]$, which agrees with the analytical result in Appendix. For $b = +2.7\pi$ [see Fig. 5(b)], hysteresis occurs in the range between $\tau_-(1)$ and the saddle-node bifurcation curve for in-phase synchronized periodic orbits for K values other than $K = 5$ used in Figs. 2(b) and 3(b). For $b = -4.0\pi$ [see Fig. 5(c)], hysteresis occurs in the range between $\tau_+(0)$ and the saddle-node bifurcation curve for antiphase synchronized periodic orbits.

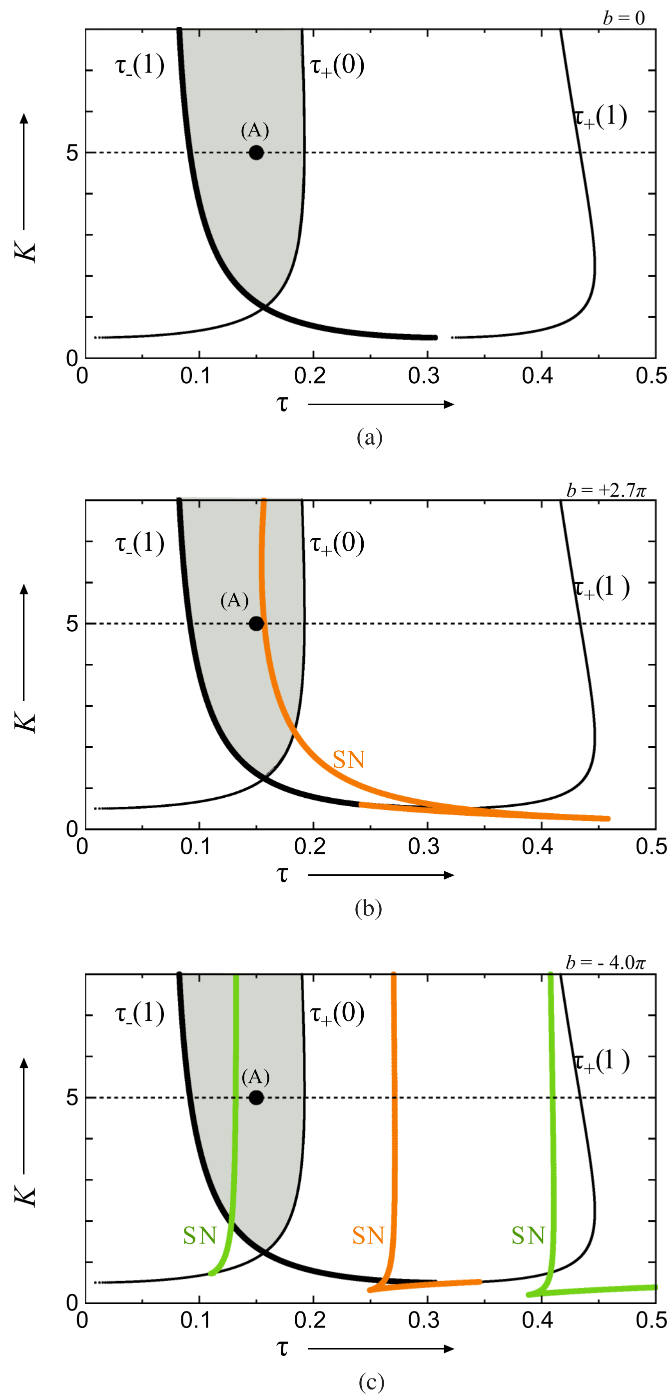

FIG. 5. Bifurcation curves and stable region for equilibrium point (4) in coupling parameter space (τ, K) with $\omega = 10$ for (a) $b = 0$, (b) $b = +2.7\pi$, and (c) $b = -4.0\pi$. The bold (thin) black lines represent the Hopf bifurcation curves $\tau_-(\ell)$ [$\tau_+(\ell)$] analytically obtained using Eq. (7). The orange (green) lines represent the saddle-node (denoted SN) bifurcation curves for in-phase (antiphase) synchronized periodic orbits, which were derived using the procedure described in Sec. V. The gray area is the stable region for equilibrium point (4).

Note that the bifurcation curves and stable region obtained above provide information for selecting coupling parameters

[3] A previous study [58] derived the bifurcation curves for a delayed feedback control system consisting of a single SL oscillator (1) and a delayed feedback controller. The present study extends the results of that study to a pair of oscillators in consideration of the synchronized state (in phase or antiphase).

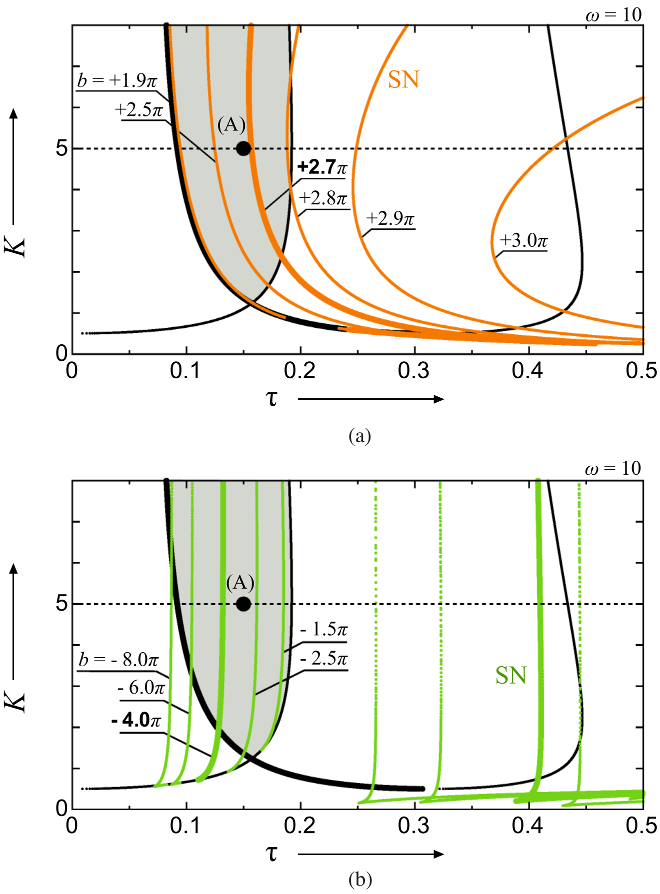

FIG. 6. Saddle-node bifurcation curves for in-phase (i.e., orange lines) and antiphase (i.e., green lines) synchronized periodic orbits in coupling parameter space (τ, K) with the fixed nominal value $\omega = 10$ for (a) $b \in \{+1.9\pi, +2.5\pi, +2.8\pi, +2.9\pi, +3.0\pi\}$ (thin orange lines) around the nominal value $b = +2.7\pi$ (bold orange line) and (b) $b \in \{-8.0\pi, -6.0\pi, -2.5\pi, -1.5\pi\}$ (thin green lines) around the nominal value $b = -4.0\pi$ (bold green line). The bold and thin black lines and the gray area are the same as in Fig. 5.

(τ, K) that avoid synchronized periodic orbits, which prevent AD from occurring, as shown in Fig. 1. To induce AD without fail, (τ, K) have to be chosen from the stable range for τ except the hysteresis range.

The bifurcations curves investigated above are based on only the specific values $\omega = 10$, $b = +2.7\pi$, and $b = -4.0\pi$. We now consider the dependency of these curves on ω and b: the specific values are used as the nominal values. First, for the fixed nominal value $\omega = 10$, the parameter b is set to values around the nominal values of $b = +2.7\pi$ and $b = -4.0\pi$. Figure 6(a) shows the saddle-node bifurcation curves for in-phase orbits for $b \in \{+1.9\pi, +2.5\pi, +2.8\pi, +2.9\pi, +3.0\pi\}$ (thin orange lines) around the nominal value $b = +2.7\pi$ (bold orange line). Figure 6(b) shows the curves for antiphase orbits for $b \in \{-8.0\pi, -6.0\pi, -2.5\pi, -1.5\pi\}$ (thin green lines) around the nominal value $b = -4.0\pi$ (bold green line). As can be seen, in both Figs. 6(a) and 6(b), increasing b causes the curves to shift to the right. Next, for fixed nominal values of $b = +2.7\pi$ and $b = -4.0\pi$, the parameter ω is set to values around the nominal value $\omega = 10.0$. The Hopf bifurcation

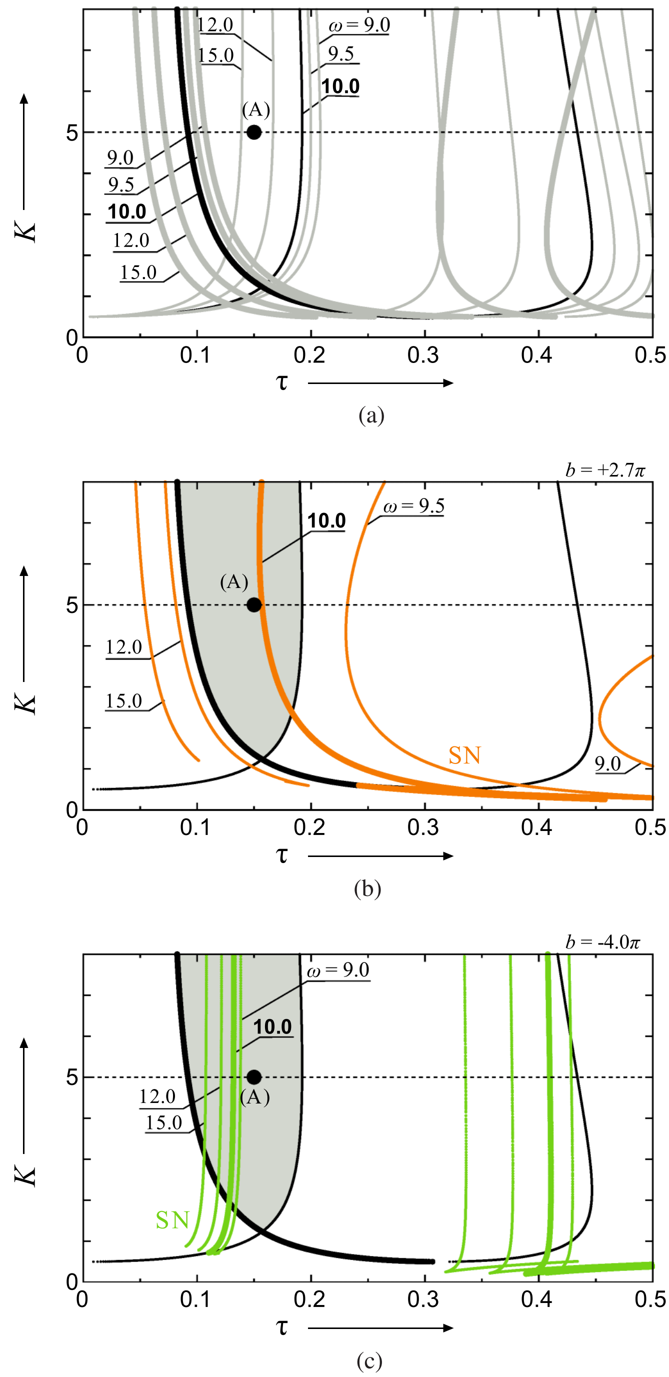

FIG. 7. Bifurcation curves in coupling parameter space (τ, K) for $\omega \in \{9.0, 9.5, 12.0, 15.0\}$ around the nominal value $\omega = 10.0$. (a) Hopf bifurcation curves for $\omega \in \{9.0, 9.5, 12.0, 15.0\}$ (gray lines) around $\omega = 10.0$ (black line). Saddle-node bifurcation curves for in-phase (orange lines) and antiphase (green lines) synchronized periodic orbits for (b) $\omega \in \{9.0, 9.5, 12.0, 15.0\}$ (thin orange lines) around $\omega = 10.0$ (bold orange line) with $b = +2.7\pi$ and (c) $\omega \in \{9.0, 12.0, 15.0\}$ (thin green lines) around $\omega = 10.0$ (bold green line) with $b = -4.0\pi$. The bold and thin black lines and the gray area are the same as in Fig. 5.

curves for equilibrium point (4) for $\omega \in \{9.0, 9.5, 12.0, 15.0\}$ (gray lines) around $\omega = 10.0$ (black line) are plotted in Fig. 7(a). It can be seen that the Hopf bifurcation curves shift to the left with increasing ω, which is reasonable based on Eq. (7). Figure 7(b) shows the saddle-node bifurcation curves for in-phase orbits for $\omega \in \{9.0, 9.5, 12.0, 15.0\}$ (thin orange lines) around $\omega = 10.0$ (bold orange line) with the fixed nominal value $b = +2.7\pi$. Figure 7(c) shows the curves for antiphase orbits for $\omega \in \{9.0, 12.0, 15.0\}$ (thin green lines) around $\omega = 10.0$ (bold green line) with the fixed nominal value $b = -4.0\pi$. In both Figs. 7(b) and 7(c), it can be seen that increasing ω causes the saddle-node bifurcation curves to shift to the left.

VI. DISCUSSION

This section briefly compares the present study with a previous study [59] that dealt with not only the local stability of delay-induced AD but also the behavior of periodic orbits. Furthermore, we discuss the open questions that remain.

The previous study [59] considered the situation where oscillators with a stable equilibrium point, an unstable periodic orbit, and a stable periodic orbit are coupled via a time-delay connection. It was shown that the delay coupling can induce the disappearance of these periodic orbits via saddle-node bifurcation by increasing the coupling strength. In contrast, the present study focuses on the situation where oscillators with an unstable equilibrium point and only a stable periodic orbit are coupled via a time-delay connection. The bifurcation diagrams and the bifurcation curves demonstrated that the delay coupling can induce the coexistence of a stable equilibrium point, an unstable periodic orbit, and a stable periodic orbit.

To gain initial insight into the global dynamics of delay-induced AD, the present study focused on only the simplest case where two identical SL oscillators are coupled via a simple delay connection. The obtained results are thus insufficient for practical situations. More complicated cases, such as those involving networks consisting of three or more oscillators and frequency mismatch, should be considered in future work.

VII. CONCLUSIONS

This study investigated the global dynamics of AD in delay-coupled identical SL oscillators whose frequency depends on amplitude. Bifurcation diagrams, which plotted the synchronized periodic orbits and the equilibrium point (with information on their stability), clarified the mechanism of the emergence of delay-induced AD from the viewpoint of global dynamics. This mechanism indicates that for the situation where the delay time for connections is continuously varied, explosive AD emerges via a Hopf bifurcation of the equilibrium point and a saddle-node bifurcation of in-phase or antiphase synchronized periodic orbits. The Hopf and saddle-node bifurcation curves in the coupling parameter space revealed the relation between the coupling parameters and the global dynamics of AD.

ACKNOWLEDGMENT

This study was supported in part by JSPS KAKENHI (JP21H03513 and JP23K21705).

APPENDIX: CASE OF $b = 0$ AND $\tau \in [0, 1)$

For $b = 0$, to eliminate $\cos \Omega\tau \cos m\pi$, substituting Eq. (17) into Eq. (11a) yields

$$R^2 = 1 - K - \frac{1}{\tau}. \tag{A1}$$

We note that R^2 is negative if $K > \tau - 1$ holds; therefore, saddle-node bifurcation does not occur for $K > \tau - 1$. This guarantees that this bifurcation (i.e., explosive AD) never occurs (i.e., $R^2 < 0$) for any $\tau \in [0, 1)$ under $b = 0$ and $K \geqslant 0$, which agrees with the bifurcation diagram in Fig. 2(a) and the bifurcation curves in Fig. 5(a).

[1] M. Frasca, L. V. Gambuzza, A. Buscarino, and L. Fortuna, *Synchronization in Networks of Nonlinear Circuits* (Springer, Cham, 2018).
[2] S. Boccaletti, A. N. Pisarchik, C. I. del Genio, and A. Amann, *Synchronization* (Cambridge University Press, Cambridge, 2018).
[3] A. Koseska, E. Volkov, and J. Kurths, Phys. Rep. **531**, 173 (2013).
[4] G. Saxena, A. Prasad, and R. Ramaswamy, Phys. Rep. **521**, 205 (2012).
[5] W. Zou, D. V. Senthilkumar, M. Zhan, and J. Kurths, Phys. Rep. **931**, 1 (2021).
[6] R. I. Sujith and S. A. Pawar, *Thermoacoustic Instability* (Springer, Cham, 2021).
[7] T. Biwa, S. Tozuka, and T. Yazaki, Phys. Rev. Appl. **3**, 034006 (2015).
[8] K. Moon, Y. Guan, L. K. B. Li, and K. T. Kim, Chaos **30**, 023110 (2020).
[9] H. Hyodo, M. Iwasaki, and T. Biwa, J. Appl. Phys. **128**, 094902 (2020).
[10] D. Premraj, K. Manoj, S. A. Pawar, and R. I. Sujith, Nonlinear Dyn. **103**, 1439 (2021).
[11] M. H. Doranehgard, V. Gupta, and L. K. B. Li, Phys. Rev. E **105**, 064206 (2022).
[12] Y. Liao, Y. Guan, P. Liu, K. Moon, and K. T. Kim, Nonlinear Dyn. **112**, 6897 (2024).
[13] S. R. Huddy and J. D. Skufca, IEEE Trans. Power Electron. **28**, 247 (2013).
[14] R. E. Mirollo and S. H. Strogatz, J. Stat. Phys. **60**, 245 (1990).
[15] D. Aronson, G. Ermentrout, and N. Kopell, Physica D **41**, 403 (1990).
[16] Y. Sugitani and K. Konishi, Nonlinear Theor. Appl., IEICE **12**, 612 (2021).
[17] D. V. Ramana Reddy, A. Sen, and G. L. Johnston, Phys. Rev. Lett. **80**, 5109 (1998).
[18] D. Ramana Reddy, A. Sen, and G. Johnston, Physica D **129**, 15 (1999).
[19] D. V. Ramana Reddy, A. Sen, and G. L. Johnston, Phys. Rev. Lett. **85**, 3381 (2000).
[20] W. Zou, Y. Tang, L. Li, and J. Kurths, Phys. Rev. E **85**, 046206 (2012).
[21] Y. N. Kyrychko, K. B. Blyuss, and E. Schöll, Philos. Trans. R. Soc. A **371**, 20120466 (2013).

[22] Y. Sugitani, K. Konishi, and N. Hara, Phys. Rev. E **92**, 042928 (2015).
[23] R. M. Nguimdo, Phys. Rev. E **97**, 032211 (2018).
[24] A. Otto, G. Radons, D. Bachrathy, and G. Orosz, Phys. Rev. E **97**, 012311 (2018).
[25] A. Sharma, Phys. Lett. A **383**, 1865 (2019).
[26] A. Ghosh, S. Mondal, and R. I. Sujith, Chaos **32**, 101106 (2022).
[27] S. R. Huddy and J. Sun, Phys. Rev. E **93**, 052209 (2016).
[28] S. R. Huddy, Chaos **30**, 013118 (2020).
[29] M. P. Mehta and A. Sen, Phys. Lett. A **355**, 202 (2006).
[30] Y. Sugitani, K. Konishi, L. B. Le, and N. Hara, Chaos **24**, 043105 (2014).
[31] N. Zhao and Z. Sun, Int. J. Bifurcation Chaos **30**, 2050094 (2020).
[32] W. Zou, Y. Chen, D. V. Senthilkumar, and J. Kurths, Chaos **32**, 041102 (2022).
[33] K. Konishi, K. Yoshida, Y. Sugitani, and N. Hara, Phys. Rev. E **109**, 014220 (2024).
[34] Y. Sugitani, K. Kawahara, and K. Konishi, Phys. Rev. E **109**, 064213 (2024).
[35] R. Dodla, A. Sen, and G. L. Johnston, Phys. Rev. E **69**, 056217 (2004).
[36] A. E. Biju, S. Srikanth, K. Manoj, S. A. Pawar, and R. I. Sujith, Nonlinear Dyn. **112**, 11329 (2024).
[37] H. Bi, X. Hu, X. Zhang, Y. Zou, Z. Liu, and S. Guan, Europhys. Lett. **108**, 50003 (2014).
[38] U. K. Verma, A. Sharma, N. K. Kamal, J. Kurths, and M. D. Shrimali, Sci. Rep. **7**, 7936 (2017).
[39] N. Zhao, Z. Sun, X. Yang, and W. Xu, Phys. Rev. E **97**, 062203 (2018).
[40] R. Ghosh, U. K. Verma, S. Jalan, and M. D. Shrimali, Phys. Rev. E **108**, 044207 (2023).
[41] M. P. Asir, P. Durairaj, S. Kanagaraj, and M. Lakshmanan, Chaos, Solitons Fractals **182**, 114741 (2024).
[42] U. K. Verma, A. Sharma, N. K. Kamal, and M. D. Shrimali, Phys. Lett. A **382**, 2122 (2018).
[43] U. K. Verma, A. Sharma, N. K. Kamal, and M. D. Shrimali, Chaos **29**, 063127 (2019).
[44] C. Liu, C. Zhou, J. Wang, C. Fietkiewicz, and K. A. Loparo, IEEE Trans. Cybern. **51**, 5046 (2021).
[45] U. K. Verma, S. S. Chaurasia, and S. Sinha, Phys. Rev. E **100**, 032203 (2019).
[46] S. Dixit, S. Nag Chowdhury, D. Ghosh, and M. Dev Shrimali, Europhys. Lett. **133**, 40003 (2021).
[47] K. Sathiyadevi, D. Premraj, T. Banerjee, and M. Lakshmanan, Phys. Rev. E **106**, 024215 (2022).
[48] S. Liu, Z. Sun, L. Yan, N. Zhao, and W. Xu, Nonlinear Dyn. **110**, 2741 (2022).
[49] J. Wang, C. Gu, and P. Ji, New J. Phys. **24**, 073038 (2022).
[50] S. Liu, Z. Sun, N. Zhao, and W. Xu, Int. J. Bifurcation Chaos **32**, 2250018 (2022).
[51] S. Liu, Z. Sun, Y. Miao, N. Zhao, and W. Xu, Chaos, Solitons Fractals **166**, 112961 (2023).
[52] N. Hui, D. Biswas, B. Bandyopadhyay, M. Chakraborty, and T. Banerjee, Chaos, Solitons Fractals **181**, 114713 (2024).
[53] Y. Kuramoto, *Chemical Oscillations, Waves, and Turbulence* (Springer, Berlin, Heidelberg, 1984).
[54] R. C. Hinz, P. Hövel, and E. Schöll, Chaos **21**, 023114 (2011).
[55] S. Mizukami, K. Konishi, Y. Sugitani, T. Kouda, and N. Hara, Phys. Rev. E **104**, 054207 (2021).
[56] T. Iwamoto, Y. Sugitani, S. Masamura, K. Konishi, and N. Hara, Phys. Rev. E **102**, 032206 (2020).
[57] D. Breda, S. Maset, and R. Vermiglio, *Stability of Linear Delay Differential Equations* (Springer, New York, NY, 2015).
[58] W. Just, B. Fiedler, M. Georgi, V. Flunkert, P. Hövel, and E. Schöll, Phys. Rev. E **76**, 026210 (2007).
[59] F. M. Atay, Physica D **183**, 1 (2003).